Lawrence Berkeley National Laboratory

Title

3D Mechanical Analysis of a Compact ${\text{Nb}}_{\text{3}}{\text{Sn}}$ IR Quadrupole for EIC

Permalink

Journal

ISSN

Authors

Vallone, Giorgio
Anerella, Michael
Parker, Brett
et al.

Publication Date

DOI

3D Mechanical Analysis of a Compact Nb$_3$Sn IR Quadrupole for EIC

Giorgio Vallone [ID], Michael Anerella, Brett Parker, John Cozzolino, Timothy Michalski, Stephen Plate,
Soren Prestemon [ID], *Senior Member, IEEE*, GianLuca Sabbi [ID], and Jesse Schmalzle

Abstract—**The Electron Ion Collider (EIC) will require large aperture quadrupole magnets for the Hadron beam in the insertion region. Key requirements include high field, compact size, and tight control of the fringe fields. A 120 mm aperture, 308.4 mm outer diameter actively shielded Nb$_3$Sn quadrupole model is under development to support these goals. This work is being carried out by a collaboration of BNL, JLAB and LBNL. A compact shell-based structure preloaded with a bladder and key system was developed for this project. In this paper, the effect of the compact structure on the mechanical behavior was investigated. In particular, the impact of the assembly tolerances and coil size variations on the actual coil stresses and bladder pressures was computed and compared with results from larger bladder and key structures developed for the LHC IR. The longitudinal preload is provided by stainless steel rods. Differently from other bladder and key magnets, the rods are first preloaded axially before coil axial load is applied. This new design aims to increase the overall stiffness of the system and reduce the longitudinal coil displacement during powering. Based on the results of a 3D mechanical analysis, the preliminary pre-load targets for the EIC quadrupole assembly will be reviewed and discussed.**
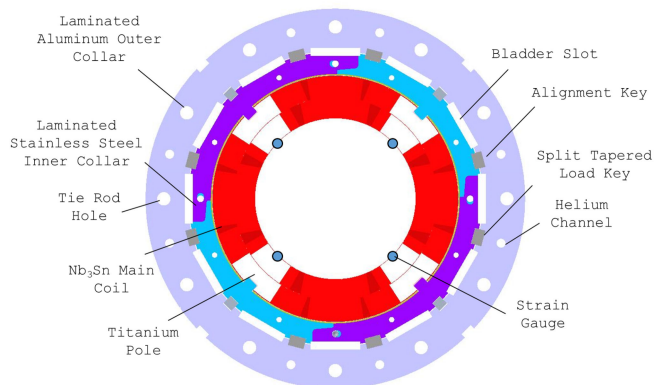
.

Fig. 1. One octant view of the magnet cross-section, showing the location of the electrical strain gauges.

I. INTRODUCTION

A compact Nb$_3$Sn quadrupole is being developed as a part of the Electron Ion Collider (EIC) R&D Program [1].
The collider will require high gradient quadrupole superconducting magnets for the Hadron beam in the insertion region. The available space for the installation of these magnets is very small, compared to past superconducting quadrupoles design. As a consequence, there is no space for a traditional iron yoke. Moreover, as the magnets will be installed in close proximity to the electron beam, the magnetic field must be contained within the magnet. The solution for this will be the installation of an additional shielding quadrupole winding, in NbTi, on the outside of the superconducting magnet, as first proposed in [2].

In order to avoid the large cost associated with fabricating new Nb$_3$Sn coils, the magnet design was based on a set of coils developed in the past as a part of the LARP program for the HQ magnet [3]. One coil was cut in sections and used in an assembly of a short mock-up, that was assembled in order to verify the mechanical models and test the mechanical performances. Strain gauges were installed on the winding poles allowing to verify the amount of prestress applied to the windings. Four additional HQ01 coils were retrieved by BNL for assembly in the new EIC structure. The magnet targets, at 4.5 K, a field gradient of 126.5 T/m, with a peak field of 8.7 T. The design current is equal to 13.6 kA for the HQ coil, and 705 A for the shield coil.

This paper presents a mechanical analysis of the magnet, studying the azimuthal and longitudinal behavior by means of 3D FE models, and comparing the results with the available measurements. These studies were focused on the study of the impact of the reduced dimensions of the magnet structure, and on the performances of a novel longitudinal loading solution.

II. MAGNET DESCRIPTION

The magnet cross-section is shown in Fig. 1: the superconducting coils from HQ are held in place by the inner collars, made of stainless steel laminations; these are contained in a laminated outer collar made of aluminum, and by a 12 mm thick stainless steel support tube. The external radius of the magnet is equal to
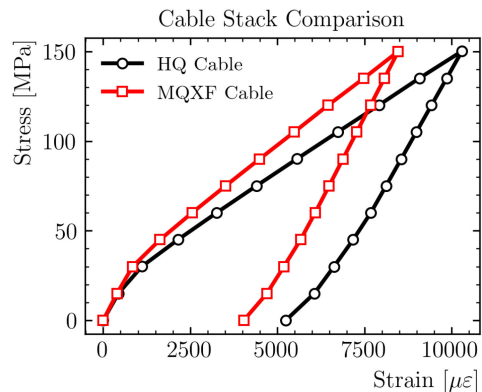
Fig. 2. Results from the 2D cable model: strain and stress averaged over the entire cable for the HQ (EIC) cable and the MQXF cable. The stiffness of the HQ cable is 10% lower.
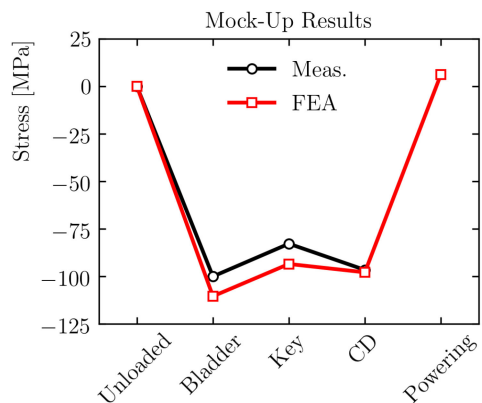

Fig. 3. Comparison between the measured and computed azimuthal stress at the winding pole strain gauge location. The points represent the stress during the bladder operation, after key insertion, after cool-down at 77 K and during powering (only FEA).

154.4 mm. For comparison, the HQ outer radius was equal to 285 mm. This leaves no space to install a sufficiently large iron yoke to return the magnetic flux. Therefore, on the outside of the magnet, a shielding quadrupole with superconducting elements in NbTi, will be installed in order to reduce the fringe field.

The magnet is loaded at room temperature by means of the bladder and key technology [4]. The water-pressurized bladders and the loading keys are inserted between the inner and outer collars. The loading keys are tapered in an attempt of minimizing the amount of clearance necessary to insert them between the collars. The outer collar is in aluminum in order to increase, or at least maintain, the azimuthal prestress during the cooldown to cryogenic temperatures. The effect of this component is expected to be smaller with respect to other conventional bladder and key magnets, which can benefit of the differential thermal contraction between the outer aluminum shell and the iron yoke. The impact of the shield coil is not considered in this study.

III. AZIMUTHAL PRE-STRESS STUDY

A. Cable Mechanical Analysis

A model of the cable was created following the modeling strategy presented in [7]. This modeling strategy allows to estimate the stiffness and thermal contraction of superconducting coils by simulating cable stacks. The model was updated with the strand and cable parameters presented in Table I. The same parameters for the MQXF magnet are presented for comparison [5]. The results from the simulation of cable stacks under transversal pressure is shown in Fig. 2: the model reproduces the elastic and plastic phases of the loading, and the unloading. The stiffness of the HQ cable is lower in all cases: one of the key drivers of this behavior is the odd number of strands of the HQ cable.

The results of the analysis are summarized in Table II. The thermal contraction computed from the MQXF cable is equal to

4.2 mm/m, the one of the HQ magnet cable is instead 3.8 mm/m. This reduced contraction is due to the smaller insulation thickness. In relative terms, this means that both the contraction and the stiffness of the HQ cable are 10% lower than the ones of the MQXF cable.

B. Azimuthal Loading Analysis

A short mechanical mock-up, made with sections cut from an HQ coil, was assembled and loaded. Electrical strain gauges, installed on the winding poles, allowed to measure the applied force on the windings. It was showed in the past that this measurement is representative of the coil stress at the inner radius of the inner layer, which is the first location to undergo unloading during powering [8].

The measurements and the computed values are shown in Fig. 3. The average measured stress during bladder operation is equal to 99 MPa. The computed stress is higher, and equal to 110 MPa. The overshoot is contained, and the average measured stress after key insertion is equal to 83 MPa. The difference between simulation and measurements is the same during the bladder and key steps. During cooldown at cryogenic temperature, the difference becomes negligible. This might suggest that there is some frictional effect that is locking the magnet
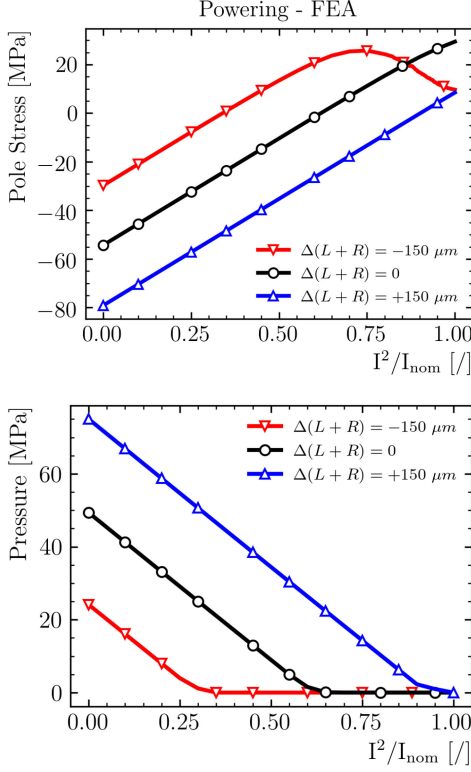
Fig. 4. Computed pole stress (top) and contact pressure between the winding pole and the coil at the inner radius (bot) during magnet powering considering the impact of an imperfect coil pack.
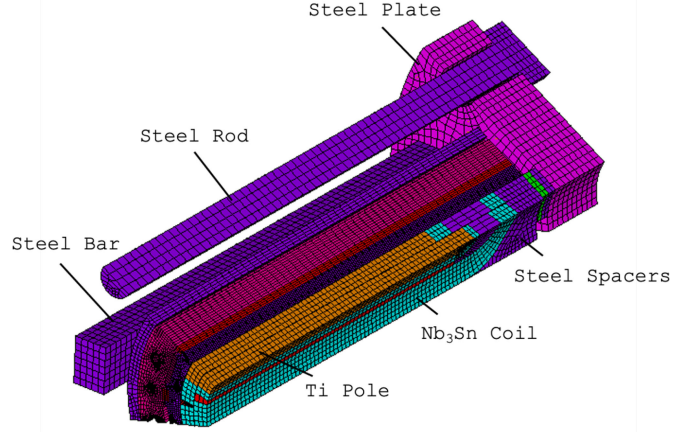

Fig. 5. 3D mechanical model showing the main components of the longitudinal loading system: the steel rods, prestressed at room temperature against the coil pack and the steel bars, and the end-plate in steel.
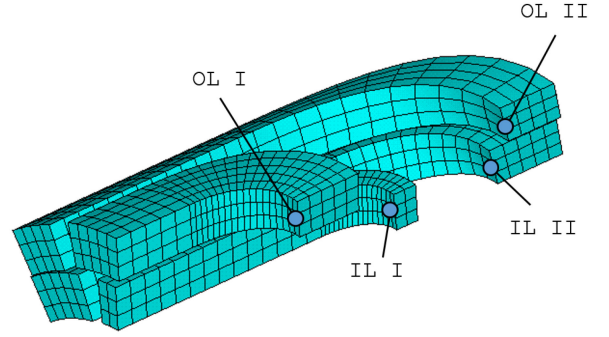

Fig. 6. Longitudinal locations selected to study the status of the coil to pole and coil to end-spacer contact status.

in a different position, and that this effect is resolved during cooldown. The computed reduction of stress due to powering is equal to 104 MPa when computed in the 3D model, 85 MPa with the 2D model. This discrepancy was observed also in MQXF models. Experimental measurements suggests that the 2D models are able to predict precisely the stress variation [9].

C. Coil-Size Impact Analysis

Coil size measurements often show substantial variations between coils and along each coil length. Metrology studies suggest that there is no strong influence of the coil total size on the local size deviations: the actual dispersion of the coil size seems more due to the fabrication tolerances of the tooling [10]. Part of the impact of these dimensional errors can be corrected with radial and mid-plane shims [11]. These corrections can be performed only on the average coil size. Therefore, local coil size variations can change the local stress status, increasing or decreasing it. In [12], it was shown that the stress variation is proportional to the coil stiffness, and the percentage of azimuthal length variation. The latter is larger for the MQXF coils, whose aperture is 150 mm, with respect to the HQ ones, whose aperture is 90 mm. As a consequence, the same size variation should bring a bigger impact on HQ coils with respect to the MQXF ones. However, it was also noticed that the structure rigidity can play a key role: a soft structure will be able to accommodate coil size variations with reduced stress variations.

Fig. 4 shows the evolution of the winding pole stress and of the contact pressure at the pole/coil interface during powering

of the EIC quadrupole. Three separate curves are provided as a function of the dimensional error of the coil, defined as the deviation of the azimuthal length of the coil $(L + R)$ from the average. A coil 150 μm smaller will see an azimuthal prestress at the pole 25 MPa lower. The contact pressure plot shows that this reduction in prestress can cause unloading, and detachment, at the interface. For comparison, the MQXF coils would experience a prestress reduction of 30 MPa for the same size variation: the reduced stiffness of the EIC quadrupole structure, and the reduced coil modulus dominate the coil stiffness increase due to the reduced radius.

IV. END-REGION ANALYSIS

The longitudinal loading system configuration is shown in Fig. 5: the magnet is prestressed with stainless steel rods, connected to a plate that presses both the coil, via set screws, and the longitudinal steel bars. This combination aims at providing the desired pressure by means of the rods, and the required stiffness with the bars. The longitudinal prestress is applied in two phases: first, the rods are engaged against the bars. Then, a torque is applied on the set screws to apply the load on the coils.

The contact pressure between the coil and the pole or the end-spacers was computed at the locations shown in Fig. 6. The values after loading, cooldown, and powering are shown in
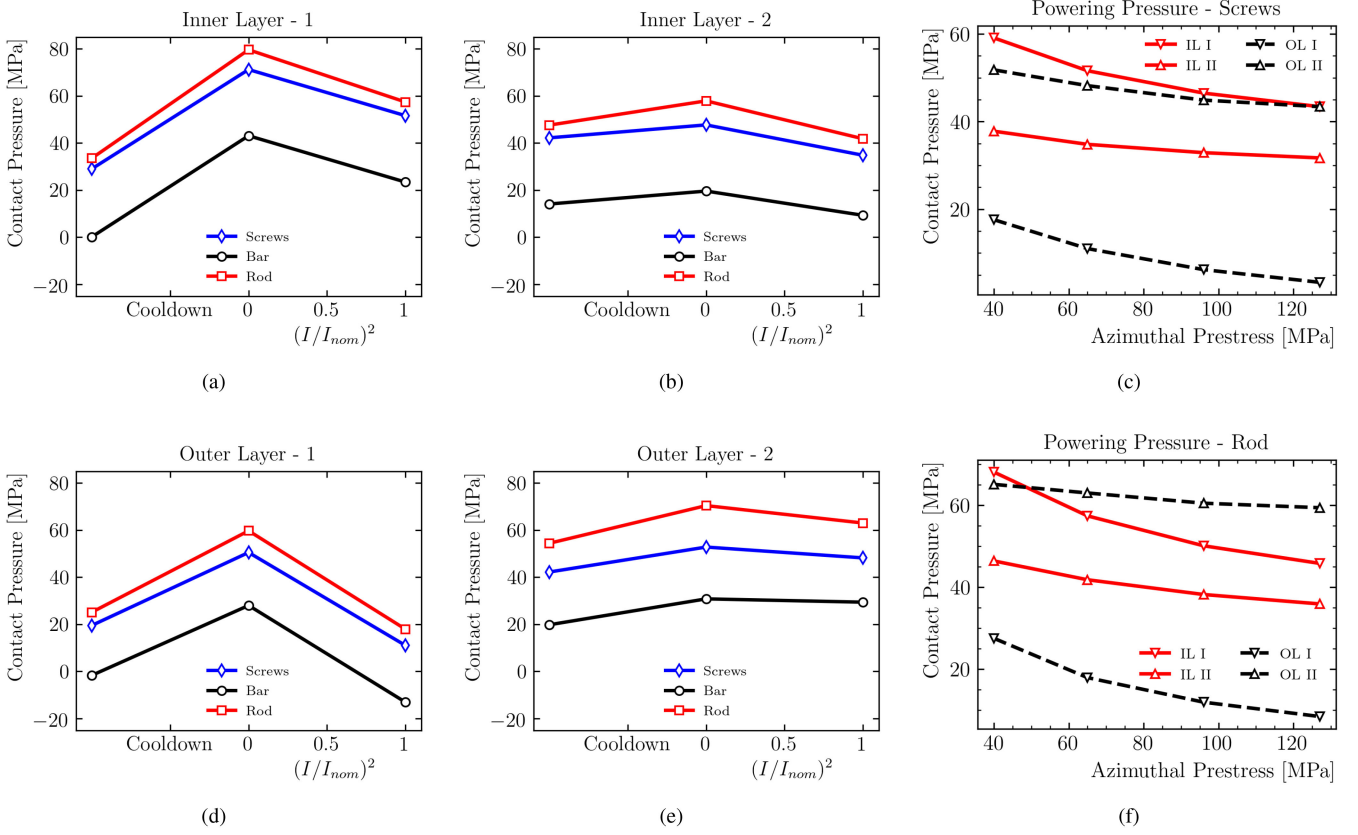
Fig. 7. Pressure at the contact locations shown in Fig. 6: (a) IL I, (b) IL II, (d) OL I, (e) OL II. Interaction between the azimuthal loading system and the longitudinal one: contact pressure at nominal current with the bar system (c) and without it (f).

Fig. 7. Ideally, the loading system would keep sufficient pressure on the coil to prevent debonding. Three cases are considered: bars installed and torque applied on the set screws (*Screws*), bars installed with no torque applied on the set screws (*Bar*), no bars installed (*Rod*). The limiting factor for the prestress is the allowed stress in the rod at room temperature, that was kept every case equal to 80% of the yield stress. The results show that the bar reduces the absolute value of the pressure applied on the coils. On the other hand, the bar system reduces the pressure variation during powering on the outer locations shown in plots (b) and (e). This, however, does not prevent a resulting tension in the contact between the outer layer of the coil pole turn for the *Bar* case.

Another performance index is the total displacement during powering: a lower displacement should reduce the total longitudinal slipping, avoiding heat releases that might result in quenches. The rod strain increase during powering is equal to 35 μm when the bar is used and 88 μm when the bar is not there. This means that the total elongation of the magnet, and the related displacements, are more than two times lower when the bar system is used.

A. Azimuthal Prestress Interaction

Friction plays a critical role in the amount of longitudinal force that can reach the coil ends. As a consequence, the amount of azimuthal prestress applied to the magnet can affect the

longitudinal behavior of the magnet. To minimize this impact, in the past different loading procedures were considered, for example applying gradually the prestress azimuthally and longitudinally gradually, in an alternate fashion. Here, for simplicity, the longitudinal prestress is applied only after the azimuthal loading operation. Fig. 7(c) and (f) show the contact pressure at nominal current, as a function of the azimuthal prestress previously applied. As the azimuthal prestress increases, the amount of available longitudinal prestress decreases. The results suggest that the effect is almost identical for the different systems considered.

V. Conclusion

This paper studied the mechanical design and performances of a compact Nb_3Sn quadrupole magnet for EIC. A cable model was used to compute the stiffness and thermal contraction of the coils. The obtained values allowed to obtain a good agreement between the measured and computed coil stresses during the loading operation and after cooldown. The applied prestress is affected by the coil size: a size variation of ± 150 μm corresponds to ± 25 MPa at the pole.

The novel longitudinal loading system introduced in the magnet uses steel bars to provide additional longitudinal stiffness to the magnet. This reduces the longitudinal displacements during powering, but reduces the contact pressure between the coil and the end-spacers.

References

[1] K. Jones *et al.*, "Report of the community review of EIC accelerator R&D for the office of nuclear physics," Feb. 2017. [Online]. Available: https://science.osti.gov/-/media/np/pdf/Reports/Report_of_the_Community_Review_of_EIC_Accelerator_RD_for_the_Office_of_Nuclear_Physics_20170214.pdf?la=en&hash=1732605221E742A0A8410111195B7D6B937EAFB7

[2] B. Parker *et al.*, "The superconducting magnets of the ILC beam delivery system," in *Proc. IEEE Part. Accel. Conf.*, 2007, pp. 3196–3198.

[3] H. Felice *et al.*, "Design of HQ—A high field large bore Nb_3Sn quadrupole magnet for LARP," *IEEE Trans. Appl. Supercond.*, vol. 19, no. 3, pp. 1235–1239, Jun. 2009.

[4] S. Caspi *et al.*, "The use of pressurized bladders for stress control of superconducting magnets," *IEEE Trans. Appl. Supercond.*, vol. 11, no. 1, pp. 2272–2275, Mar. 2001.

[5] P. Ferracin *et al.*, "Development of MQXF: The Nb_3Sn low-β quadrupole for the HiLumi LHC," *IEEE Trans. Appl. Supercond.*, vol. 26, no. 4, Oct. 2016, Art. no. 4000207.

[6] H. Felice *et al.*, "Impact of coil compaction on Nb_3Sn LARP HQ magnet," *IEEE Trans. Appl. Supercond.*, vol. 22, no. 3, Feb. 2012, Art. no. 4001904.

[7] G. Vallone, B. Bordini, and P. Ferracin, "Computation of the reversible critical current degradation in Nb_3Sn Rutherford cables for particle accelerator magnets," *IEEE Trans. Appl. Supercond.*, vol. 28, no. 4, Sep. 2018, Art. no. 4801506.

[8] G. Vallone *et al.*, "Mechanical performance of short models for MQXF, the Nb_3Sn low-β quadrupole for the Hi-Lumi LHC," *IEEE Trans. Appl. Supercond.*, vol. 27, no. 4, Jun. 2017, Art. no. 4002906.

[9] E. Takala *et al.*, "Mechanical comparison of short models of Nb_3Sn low-β quadrupole for the Hi-Lumi LHC," *IEEE Trans. Appl. Supercond.*, vol. 31, no. 5, Aug. 2021, Art. no. 4000306.

[10] J. F. Troitino *et al.*, "Applied metrology in the production of superconducting model magnets for particle accelerators," *IEEE Trans. Appl. Supercond.*, vol. 28, no. 3, Apr. 2018, Art. no. 4002106.

[11] G. Vallone *et al.*, "Assembly of a mechanical model of MQXFB, the 7.2 m long low-β quadrupole for the high luminosity LHC upgrade," *IEEE Trans. Appl. Supercond.*, vol. 29, no. 5, Jan. 2019, Art. no. 4000605.

[12] G. Vallone *et al.*, "Summary of the mechanical performances of the 1.5 m long models of the Nb_3Sn low-β quadrupole MQXF," *IEEE Trans. Appl. Supercond.*, vol. 29, no. 5, Feb. 2019, Art. no. 4002805.